Available online at www.sciencedirect.com
SCIENCE DIRECT®
International Journal of Multiphase Flow 31 (2005) 435–451
International Journal of Multiphase Flow
www.elsevier.com/locate/ijmulflow

# Direct numerical simulation of fluid flow laden with many particles

S.H. Cho [a], H.G. Choi [b], J.Y. Yoo [c,*]

[a] *BK21 Project, Mechanical Engineering Research Division, Seoul National University, San 56-1, Shinlim-dong, Kwanak-ku, Seoul 151-742, Republic of Korea*
[b] *Department of Mechanical Engineering, Seoul National University of Technology, 172, Gongneung-2-dong, Nowon-ku, Seoul 139-743, Republic of Korea*
[c] *School of Mechanical and Aerospace Engineering, Seoul National University, San 56-1, Shinlim-dong, Kwanak-ku, Seoul 151-742, Republic of Korea*

Received 7 March 2004; received in revised form 20 January 2005

**Abstract**

Two-dimensional channel flow of fluid laden with many particles is studied by direct numerical simulation using the Navier–Stokes equation coupled with the equation of motion for respective particles. Fractional four-step method with Crank–Nicolson scheme and ALE technique is adopted for P2P1 mixed finite element formulation of the governing equations for fluid motion. The motion and distribution of particles in the fluid is virtually described and the calculated relative viscosity is compared with previous results within the limits of possibility. The effect of the ratio of channel gap to particle diameter on the relative viscosity and the tubular pinch effect are also delineated.


*Keywords:* Combined formulation; DNS; ALE; Fractional four-step method; Relative viscosity; Tubular pinch effect

* Corresponding author. Tel.: +82 2 880 7112; fax: +82 2 883 0179.
*E-mail address:* jyyoo@snu.ac.kr (J.Y. Yoo).

0301-9322/$ - see front matter © 2005 Elsevier Ltd. All rights reserved.
doi:10.1016/j.ijmultiphaseflow.2005.01.008

## 1. Introduction

The rheological behavior of concentrated suspensions which consist of Newtonian fluid or polymer melt laden with many particles has been a subject of great interest for many decades. The study of these suspensions is valuable for engineering applications such as coal-water slurries transport, sediment transport, rheology of blood, and rheology of composite materials. Although there have been many studies on rheological properties of such suspensions, there is still room for further understanding about the concentration and distribution of particles in a suspension, and the change of relative viscosity, because the flow characteristics of such suspensions are so complex.

Some achievements in the study of fluid flow laden with small particles were made in the early 20th century. A very dilute suspension of small rigid spherical particles in a Newtonian fluid can be assumed to be isotropic in structure and is characterized by an effective viscosity or relative viscosity, as proposed first by Einstein (1906):

$$\eta_r = \frac{\eta}{\eta_f} = 1 + 2.5\Phi, \tag{1}$$

where $\eta$, $\eta_r$, $\eta_f$, and $\Phi$ are the effective viscosity, the relative viscosity of the suspension, the viscosity of the suspending medium fluid, and the volume fraction, respectively. This equation shows that the effective viscosity is a function of the suspending medium fluid viscosity and the volume fraction. The effective viscosity of a dilute suspension of rigid cylinders in a viscous fluid at small particle Reynolds numbers was derived theoretically by Brady (1984) to be

$$\eta_r = \frac{\eta}{\eta_f} = 1 + 2.0\Phi. \tag{2}$$

There is no effect of particle size, nor of particle position on the change of relative viscosity, because the above theories neglected the effect of all other particles.

These equations are valid only for very dilute suspensions say with volume fraction $\Phi < 0.02$, where even the Brownian motion of an isolated particle has no influence on the velocity and stress of the fluid due to the presence of the particle itself in the bulk flow. Above this range of volume fraction, hydrodynamic interactions play major roles in changing flow characteristics, which include the interactions between the particles and the medium fluid, the interactions among the particles themselves, and the stress transfer from the wall. When hydrodynamic interactions come into play, so does the Brownian motion. These effects make their first appearances in the expression for the mean stress when the terms of $O(\Phi^2)$ are considered in the relative viscosity equation.

Through a theoretical study, Batchelor (1977) proposed the relative viscosity representing the bulk stress up to $O(\Phi^2)$ in a statistically homogeneous suspension of spheres subjected to a simple shear flow. The study showed that the theoretical value of 1.0 which equals the difference of coefficients of $\Phi^2$ in the relative viscosity equation, should be regarded as the direct contribution due to the Brownian motion. Therefore, the relative viscosities representing the suspensions with and without the effect of the Brownian motion are described by the following equations, respectively:

$$\eta_r = 1 + 2.5\Phi + 6.2\Phi^2, \tag{3}$$

$$\eta_r = 1 + 2.5\Phi + 5.2\Phi^2. \tag{4}$$

Dodd et al. (1995) obtained numerically the relative viscosity of a suspension of discs from self-diffusivity and average stresslet in Stokes shear flow. Prosperetti (2004) obtained analytically the relative viscosity of a quasi-random suspension of discs by calculating the ensemble-average velocity and pressure on the basis of the two-dimensional Stokes flow.

Kataoka et al. (1978) presented an expression for the effective viscosity of polymer melts filled with particles, which was obtained by using a cone-and-plate viscometer:

$$\eta_r = \left(1 - \frac{\Phi}{A}\right)^{-2}, \tag{5}$$

where $A$ is the packing geometry coefficient. Choi and Joseph (2001) used $A = 0.8328$ which scales $A$ into two dimension.

Some experimental studies made direct observations of the particle motion. Segre and Silberberg (1962a) examined radial displacements of the spherical rigid particles carried along in the Poiseuille flow. They employed an optical scanning device which utilized two mutually perpendicular light beams and allowed particles to pass through their intersection region. A statistical analysis of the counts of the passing particles enabled them to deduce the necessary data for investigating single particle behavior. In their experiment, the particle diameters were 0.32–1.71 mm and the overall particle concentrations ranged from 0.33 to 4 particles/cm$^3$. The suspensions were too dilute for the particles to interact with each other. However, the radial displacements of spherical particles in streaming suspensions were observed and the occurrence of a 'tubular pinch effect' were reported in the laminar flow of the suspension. It was also shown that a rigid sphere transported along in the Poiseuille flow through a tube is subject to radial forces which tend to carry it to a certain equilibrium radial position, irrespective of the initial radial position at which the sphere first entered the tube.

Several theoretical and computational studies of inertial lift force on a particle and migration of particles in the shear flow have been reported for the last decade. Cherukat and McLaughlin (1994) studied the problem of inertial lift on a moving sphere in contact with a plane wall as a perturbation of Stokes flow. Hogg (1994) investigated the inertial migration of non-neutrally buoyant spherical particles, suspended in a fluid flowing between two plane boundaries. Asmolov (1999) studied the inertial migration of small rigid sphere translating parallel to the walls within a channel flow. Dandy and Dwyer (1990) and Cherukat et al. (1999) reported computational studies of the inertial lift on a constrained sphere in linear shear flow using a finite volume formulation. Kurose and Komori (1999) carried out numerical simulations to determine the drag and lift forces on a rotating sphere in an unbounded linear shear flow.

Recently, with the advances of the computational techniques and the computing power, significant development has been made in directly solving the fluid–particle mixture problems of great complexity. Hesla (1991) proposed the combined formulation of fluid–particle problem that combines the fluid and particle equations of motion into a single coupled variational equation. This combined formulation links the fluid traction on a particle with the motion of the particle implicitly. Hu et al. (1992) developed a direct numerical simulation technique incorporating the combined formulation with a finite element method based on an unstructured mesh for the fluid–particle problem, and Hu (1996) carried out a direct simulation of flows of solid–liquid

mixtures. This technique was utilized by Patankar et al. (2001) who studied the lift-off to equilibrium position of a single circular particle in Newtonian and viscoelastic fluids, which is driven forward on the bottom of a channel by a plane Poiseuille flow. Feng and Michaelides (2003) investigated the equilibrium position of a single circular particle in a horizontal shear flow by LBM (lattice Boltzmann method). Choi and Joseph (2001) also studied the fluidization by lift of 300 circular particles in a plane Poiseuille flow.

In the present paper, we adopt the same direct numerical simulation as Choi and Joseph (2001) to examine the fluid flow laden with many particles that are large enough to neglect the Brownian motion in a two-dimensional channel. The changes of the rheological properties of the suspension caused by the interactions between the fluid and particles are considered. The effect of the ratio of channel gap to particle diameter and the distribution of particles in terms of the gapwise position are also discussed.

## 2. Governing equations

We consider a two-dimensional channel flow in which the fluid is laden with many particles, as schematically shown in Fig. 1. The suspension consists of a Newtonian medium fluid and non-deformable particles which have the same density as the fluid and are depicted as two-dimensional cylinders. Motivations for studying the two-dimensional case of a suspension of aligned cylinders are lucidly stated in a very recent study of Prosperetti (2004) who calculated the ensemble-average velocity and pressure in a periodic suspension of cylinders and from these results evaluated the particle stress on the assumption of Stokes' flow.

The governing equations for unsteady, laminar, incompressible flow are the conservation of mass and the conservation of momentum:

$$\nabla \cdot \mathbf{u} = 0, \tag{6}$$

$$\rho_f \frac{D\mathbf{u}}{Dt} = \rho_f \mathbf{f} + \nabla \cdot \tilde{\sigma}, \tag{7}$$

where $\mathbf{u}$, $\rho_f$, and $\mathbf{f}$ are the velocity vector, fluid density, and body force per unit mass, respectively. The stress tensor is given by

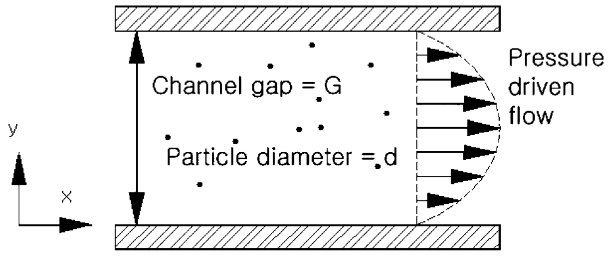


Fig. 1. A schematic of computational domain and flow condition.

$$\tilde{\sigma} = -p\tilde{\mathbf{I}} + \tilde{\tau} = -p\tilde{\mathbf{I}} + \eta_f[\nabla\mathbf{u} + (\nabla\mathbf{u})^{\mathrm{T}}], \tag{8}$$

where $\tilde{\mathbf{I}}$ and $\tilde{\tau}$ are the identity tensor and the shear stress tensor, respectively. To describe the movement of the particles, Arbitrary Lagrangian–Eulerian (ALE) technique is used so that the Navier–Stokes equation is modified as follows:

$$\rho_f\left\{\frac{\partial\mathbf{u}}{\partial t} + [(\mathbf{u} - \mathbf{u}_g)\cdot\nabla]\mathbf{u}\right\} = \rho_f\mathbf{f} + \nabla\cdot\tilde{\sigma}, \tag{9}$$

where $\mathbf{u}_g$ is the grid velocity vector which is obtained by solving the Laplace equation to guarantee its smooth variation, as adopted by Hu et al. (1992). The weak formulations of the Navier–Stokes equation and continuity equation are

$$\int_\Omega \left\{W\cdot\rho_f\left(\frac{\partial\mathbf{u}}{\partial t} + [(\mathbf{u} - \mathbf{u}_g)\cdot\nabla]\mathbf{u}\right) + \nabla W : \tilde{\sigma}\right\}\mathrm{d}\Omega - \oint_\Gamma W\cdot\tilde{\sigma}\cdot\mathbf{n}\,\mathrm{d}\Gamma = 0, \tag{10}$$

$$\int_\Omega q\nabla\cdot\mathbf{u}\,\mathrm{d}\Omega = 0, \tag{11}$$

where $W$ and $q$ are the weighting functions for the momentum and continuity equations, respectively; $\Omega$ and $\Gamma$ are the fluid domain and boundary of the fluid domain, respectively. The weighting functions can be written as follows:

$$W = w_i(\alpha_i\mathbf{e}_x + \beta_i\mathbf{e}_y),$$

$$q = \lambda_i m_i,$$

where the subscript '$i$' denotes the $i$th node; $w_i$ and $m_i$ denote the shape functions of velocity and pressure variables, respectively; $\alpha_i$, $\beta_i$ and $\lambda_i$ are arbitrary constants; $\mathbf{e}_x$ and $\mathbf{e}_y$ are the base vectors of the two-dimensional space.

The particle motion is determined by the hydrodynamic forces and described by Newton's law as follows:

$$M_n\frac{\mathrm{d}\mathbf{V}_n}{\mathrm{d}t} = \mathbf{F}_n = -\oint_{\Gamma_n}\tilde{\sigma}\cdot\mathbf{n}\,\mathrm{d}\Gamma, \tag{12}$$

for $n = 1, 2, \ldots, N$, where $M_n$, $\mathbf{V}_n$, $\mathbf{F}_n$, $\Gamma_n$, $\mathbf{n}$, and $N$ are mass of the $n$th solid particle, translational velocity vector, hydrodynamic forces, $n$th particle surface, outward unit normal vector to the particle surface, and number of particles, respectively.

The Euler equation for the angular momentum is

$$\frac{\mathrm{d}}{\mathrm{d}t}(\mathbf{I}_n\varpi_n) = \mathbf{T}_n = -\oint_{\Gamma_n}(\mathbf{x} - \mathbf{X}_n)\times(\tilde{\sigma}\cdot\mathbf{n})\,\mathrm{d}\Gamma, \tag{13}$$

where $\mathbf{I}_n$, $\varpi_n$, $\mathbf{T}_n$, $\mathbf{x}$, and $\mathbf{X}_n$ are the moment of inertia and angular velocity of the $n$th solid particle, torque acting on the particle, position vector to a point in the fluid domain, position vector to the

centroid of the $n$th particle, respectively. The centroid position, $\mathbf{X}_n$ and the orientation $\mathbf{\Theta}_n$ of the particle lead to the following relations:

$$\frac{\mathrm{d}\mathbf{X}_n}{\mathrm{d}t} = \mathbf{V}_n, \quad \frac{\mathrm{d}\mathbf{\Theta}_n}{\mathrm{d}t} = \varpi_n.$$

Using the fact that the sum of every velocity shape function is equal to 1, the hydrodynamic forces $\mathbf{F}_n$ in Eq. (12) can be written as follows:

$$\mathbf{F}_n = -\sum_{i\in\Gamma_n} \oint_{\Gamma_n} w_i(\tilde{\sigma}\cdot\mathbf{n})\,\mathrm{d}\Gamma, \tag{14}$$

where $w_i$ denotes the shape function (of the weighting function for the momentum equations) at the $i$th node point along the $n$th particle surface $\Gamma_n$. Therefore, relating Eq. (10) with Eq. (14), we can obtain the following formulation of the hydrodynamic force:

$$\mathbf{F}_n = -\sum_{i\in\Gamma_n} \int_\Omega \left\{ w_i\rho_f\left(\frac{\partial\mathbf{u}}{\partial t} + [(\mathbf{u}-\mathbf{u}_g)\cdot\nabla]\mathbf{u}\right) + \nabla w_i\cdot\tilde{\sigma}\right\}\mathrm{d}\Omega. \tag{15}$$

Thus, from Eq. (12) we can obtain the following combined formulation for the equations of motion of each particle:

$$M_n\frac{\mathrm{d}\mathbf{V}_n}{\mathrm{d}t} = -\sum_{i\in\Gamma_n} \int_\Omega \left\{ w_i\rho_f\left(\frac{\partial\mathbf{u}}{\partial t} + [(\mathbf{u}-\mathbf{u}_g)\cdot\nabla]\mathbf{u}\right) + \nabla w_i\cdot\tilde{\sigma}\right\}\mathrm{d}\Omega. \tag{16}$$

These are combined with the equation of fluid motion in a fluid–particle system, so that both the fluid and the particle equations of motion are incorporated implicitly into a single coupled equation. A similar procedure is applied to obtain a combined formulation for the angular momentum equation:

$$\frac{\mathrm{d}}{\mathrm{d}t}(\mathbf{I}_n\varpi_n) = -\sum_{i\in\Gamma_n} \int_\Omega (\mathbf{x}-\mathbf{X}_n)\times\left\{ w_i\rho_f\left(\frac{\partial\mathbf{u}}{\partial t} + [(\mathbf{u}-\mathbf{u}_g)\cdot\nabla]\mathbf{u}\right) + \nabla w_i\cdot\tilde{\sigma}\right\}\mathrm{d}\Omega. \tag{17}$$

Finally, the following kinematic constraint should be imposed on each particle surface in order to guarantee the no-slip condition:

$$\mathbf{u} = \mathbf{V}_n + \varpi_n\times(\mathbf{x}-\mathbf{X}_n). \tag{18}$$

Combining Eqs. (10), (11), (12), (17) and (18), and assembling all the elemental matrices, the global matrix is obtained:

$$\begin{bmatrix} A & B & C \\ (B)^{\mathrm{T}} & 0 & 0 \\ D & E & F \end{bmatrix}\begin{bmatrix} U \\ P \\ V \end{bmatrix} = \begin{bmatrix} f \\ 0 \\ g \end{bmatrix}. \tag{19}$$

where $A$, $B$, $C$, $D$, $E$ and $F$ are sparse matrices; $U$, $P$ and $V$ represent the vectors of the velocities, pressures, and the vectors combining all the translational velocity components ($U_n$, $V_n$) and the angular velocities ($\varpi_n$) of the solid particles; $f$ and $g$ include the external force terms in the fluid and solid momentum equations. For two-dimensional flow problems, the dimension of the vector $U$ is twice the number of nodes in the mesh, the dimension of the vector $P$ is the number

of vertices in the mesh, and the dimension of the vector $V$ is three times the number of rigid particles.

A fractional four-step method of Choi et al. (1997) with the second-order-accurate fully-implicit Crank–Nicolson time-marching scheme is used to discretize Eqs. (10) and (11) with P2P1 mixed finite element method. The ALE technique is adjusted to be applicable to body-fitted, unstructured, finite element mesh. For further details of these numerical methods, reference should be made to Choi (2000).

## 3. Results and discussions

We now investigate the two-dimensional flow of a suspension laden with many rigid cylindrical particles in a plane channel as shown in Fig. 1, where the medium fluid is Newtonian and the particles are freely dispersed in the fluid since the density of the particle is the same as that of the fluid.

The Reynolds number depends on the wall shear rate, so that it is expressed as

$$Re = \rho_f \dot{\gamma}_w d^2/\eta_f, \tag{20}$$

where $\dot{\gamma}_w$ and $d$ are the shear rate at the wall in the absence of the particles and particle diameter, respectively. Unless otherwise specified, the Reynolds number, $Re = 10$ is held fixed for all simulation cases, regardless of the channel gap considered in the present study. The pressure gradient in the channel is given as a function of the Reynolds number:

$$\frac{\Delta P}{\Delta x} = Re \cdot \frac{2\eta_f}{G} \cdot \frac{v}{d^2} = Re \cdot \frac{2\eta_f}{G} \cdot \frac{\eta_f}{d^2 \rho_f} = Re \cdot \frac{2\eta_f^2}{\rho_f G d^2}. \tag{21}$$

where $v$ is the dynamic viscosity.

The computational domain is a two-dimensional plane channel with a periodic boundary, where the ratio of channel gap to channel length ($G/L$) is about 10:63. Three different cases of the ratio of channel gap to particle diameter ($G/d$) are to be considered, that is, $G/d = 5$, 10, and 40. In the channel for $G/d = 10$, the ratio of channel length to particle diameter ($L/d$) is 63, so that the size of the calculation domain is $10d \times 63d$. This is similar to that of Choi and Joseph (2001), who used $12d \times 63d$, which was conceived to be long enough to cover the four or more of the waves of pressure pattern of the fluid motion. The volume fraction of the suspension is varied from 0.05 to 0.4 in the present study. Table 1 shows the input data for the present simulation of fluid flow laden with many particles and, as an example, the computational mesh for the case of $G/d = 5$ and $\Phi = 0.05$ is shown in Fig. 2, where the particles are initially suspended at random positions. When the pressure gradient is applied in the channel, the particles will move by hydrodynamic forces.

In order to find out the effective viscosity of the suspension, the velocity profile has to be known. However, unlike parabolic velocity profile of the purely Newtonian fluid, the velocity profile of the fluid laden with many particles cannot be known a priori because the effective viscosity changes when particles are fluidized in the fluid. Therefore, we are to calculate averaged velocities along the distance from the wall. Then the fluid laden with particles is to have a velocity profile slower than that of the corresponding Newtonian fluid because the existence of particles affect the stress field of the fluid in the sense that the velocity decreases as the volume fraction increases.

Table 1
Input data for the simulation of fluid flow laden with many particles

| Gap/diameter $G/d$ | Length/diameter $L/d$ | Volume fraction $\Phi$ | Number of particles $N$ | Reynolds number $Re$ |
|---|---|---|---|---|
| 5 | 63 | 0.05 | 20 | 10 |
| 5 | 63 | 0.10 | 40 | 10 |
| 5 | 63 | 0.20 | 80 | 10 |
| 5 | 63 | 0.30 | 120 | 10 |
| 5 | 63 | 0.40 | 160 | 10 |
| 10 | 63 | 0.05 | 40 | 10 |
| 10 | 63 | 0.10 | 80 | 0.1 |
| 10 | 63 | 0.10 | 80 | 1 |
| 10 | 63 | 0.10 | 80 | 5 |
| 10 | 63 | 0.10 | 80 | 10 |
| 10 | 63 | 0.20 | 160 | 10 |
| 10 | 63 | 0.30 | 240 | 10 |
| 10 | 63 | 0.40 | 320 | 10 |
| 40 | 252 | 0.05 | 640 | 10 |
| 40 | 252 | 0.10 | 1280 | 10 |
| 40 | 252 | 0.20 | 2560 | 10 |
| 40 | 252 | 0.30 | 3840 | 10 |
| 40 | 252 | 0.40 | 5120 | 10 |

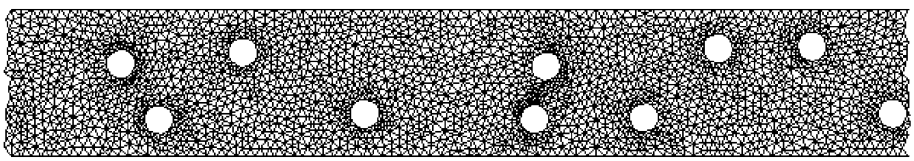

Fig. 2. Computational mesh when the fluid domain contains 10 particles ($G/d = 5$, $\Phi = 0.05$).

To validate the code, grid sensitivity test was performed by increasing the number of nodes disposed on a particle surface up to 30 at $G/d = 10$, $\Phi = 0.1$, and $Re = 10$. Fig. 3 shows averaged velocity distributions across the channel gap for various numbers of nodes on a particle surface. When the number is 6, the calculation did not reach convergence. With 10 nodes it reached convergence but there is some discrepancy between the results with 10 and 15 nodes on a particle surface. However, there is negligible difference between the results with 15 and 30 nodes. Thus, it can be said that 15 nodes on a particle surface is acceptable for the present problem.

A particle migrates in such a manner that its streamwise velocity component is much greater than its gapwise velocity component. Therefore, it takes much time for each particle to reach its equilibrium gapwise position, so that sufficient computation time is required for attaining the equilibrium state of the flow field. Fig. 4 shows the variation of particle distribution with time at $G/d = 10$, $\Phi = 0.2$ and $Re = 10$. The particle distribution is represented by $N_s/N$, where $N$ is the total number of particles in the channel and $N_s$ is the number of particles in a section which is a gapwise interval defined by dividing the channel gap by 10. Initially, the particles are distributed randomly or rather uniformly across the channel. As time goes on, the gapwise distribution of

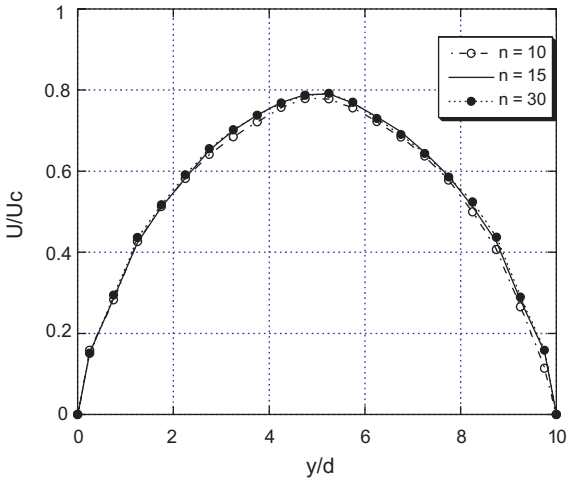


Fig. 3. Velocity profiles of the suspension with respect to the gapwise position for various grid nodes on a particle surface at $G/d = 10$, $\Phi = 0.4$, and $Re = 10$.

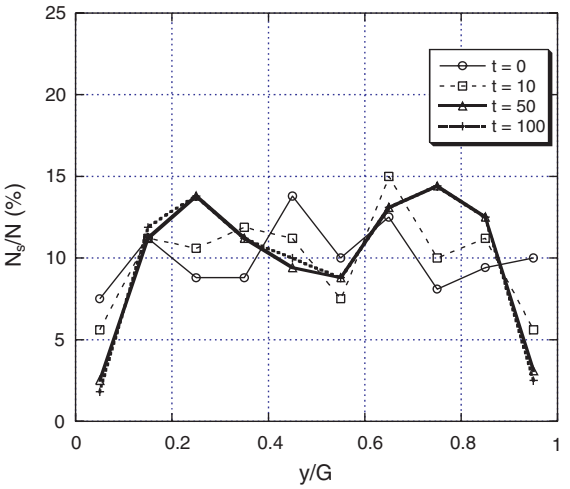


Fig. 4. Distribution of particles along the gapwise direction as time goes on at $G/d = 10$, $\Phi = 0.2$, and $Re = 10$.

particles exhibits the pinch effect with little change. Therefore, it can be said that the particle distribution of the present simulation has reached an equilibrium state. Although not shown here to save space, similar results were obtained for the case of a smaller $Re$ than that in Fig. 4 when sufficient computation time was taken together with grid convergence test.

As another code validation, the lift-off force of a single particle in a Newtonian fluid is studied. The simulation condition of this problem, $G/d = 12$, $L/d = 22$, and $Re = 6.67$, is the same as that of Patankar et al. (2001). It turns out that the migration height at which the buoyant weight balances the hydrodynamic lift is 0.78 at $Re = 6.67$, which is exactly the same as Patankar et al.

The particle positions and pressure distribution at $G/d = 10$, $\Phi = 0.4$, and $Re = 10$ are shown in Fig. 5 for the fully developed flow condition. The flow field looks complicated with dispersed particles and we cannot notice any distinctive flow patterns yet.

Now, we calculate $\eta_r$ (the relative viscosity of the suspension) in the sections designated according to the distance from the wall by the following procedure. First, hundreds of streamwise velocity $u$ are extracted across each section using TECPLOT at fully developed equilibrium state. Then, we obtain the representative velocity of each section by averaging these velocities. Knowing that the stress distribution is linear in the gapwise direction at fully developed flow condition, we are now able to obtain the effective viscosity for each section from the well-known relation between the shear stress and the velocity gradient:

$$\tau(y) = \eta(y)\frac{\mathrm{d}u}{\mathrm{d}y}, \quad \eta(y) = \tau(y)\frac{\Delta y}{\Delta u}.$$

Finally, the relative viscosity of the suspension is found by averaging these viscosities.

Fig. 6 shows the variation of the relative viscosity with volume fraction at $G/d = 40$ and $Re = 10$, in comparison with some previous works. The error bars on the data obtained by the present simulation represent the highest and lowest effective viscosities at different sections across the channel. It may not be appropriate to make direct comparisons with previous works because most of them are for different flows of different fluids under different conditions from the present study (as discussed earlier in the Introduction) which considers pressure-driven flows in two-dimensional channels on the basis of the Navier–Stokes equations. Prosperetti's (2004) result shows largest deviation from the present study which may be due to the assumption of a quasi-random suspension of discs subjected to two-dimensional Stokes flow. Kataoka et al.'s (1978) result scaled into two dimension may reflect the effect of simple shear flow of particle-laden shear-thinning polymer melt. Batchelor's (1977) result is for uniform suspension of spherical particles, where Brownian motion plays an important role. However, it should be noted that unlike the above studies particle–particle and particle–wall interactions are intrinsically included in the present DNS of flow of fluid–particle mixture, so that the resistance of the suspension to flow can be most realistically represented.

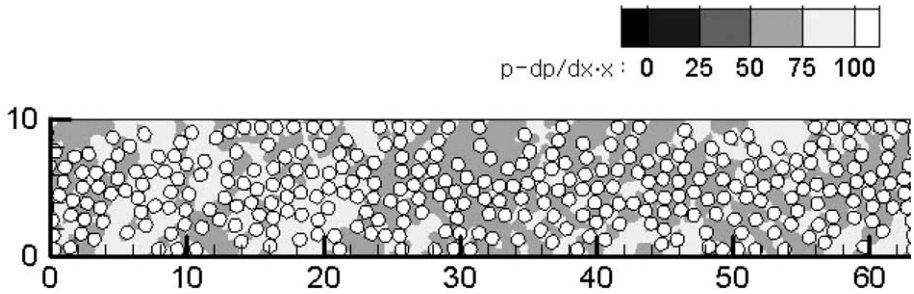


Fig. 5. Snapshot of the motion of particles and the pressure distribution when the fluid domain contains 320 particles ($G/d = 10$, $\Phi = 0.4$). The constant pressure gradient times the distance is subtracted from the pressure to represent the disturbance due to the movement of particles.

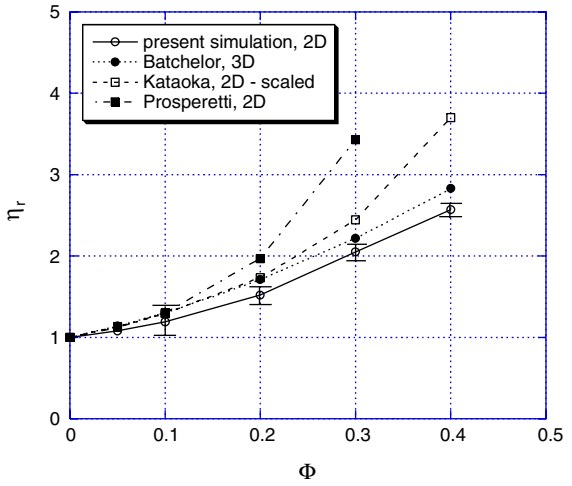


Fig. 6. Comparison of relative viscosity of solid–particle–laden Newtonian fluid with other expressions at $G/d = 40$ and $Re = 10$ for various volume fractions $\Phi$.

We now consider the effect of particle size on the fluid flow for various volume fractions by comparing the three cases, $G/d = 5, 10, 40$, at a fixed Reynolds number, $Re = 10$, as shown in Fig. 7. As the ratio of channel gap to particle diameter increases for the same volume fraction, the relative viscosity of the suspension decreases. This effect becomes more pronounced as the volume fraction of the fluid increases. At this point, it is noteworthy that the 'local' effective viscosity near the channel wall will be reduced when the particle size becomes larger since the lubrication layer (clear fluid) next to the channel wall will be proportional to the particle size. However, as the particle density reduces in the lubrication layer (as will be shown later in Fig. 10), it increases in the center region generating a stronger particle–particle interaction there. This causes a flat

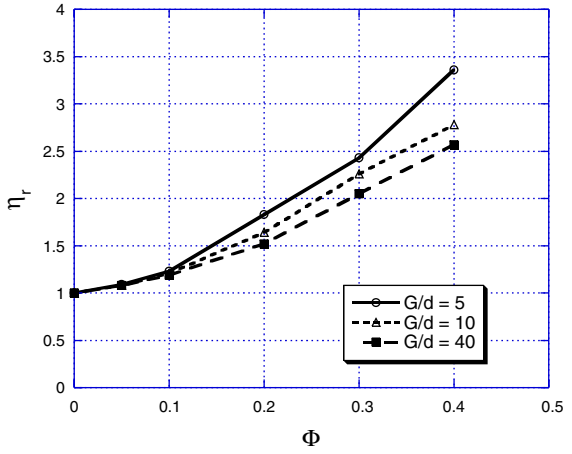


Fig. 7. Comparison of relative viscosity of particle–laden fluid for various channel gaps at $Re = 10$.

velocity profile like that of Bingham channel flow, thus explaining the steep velocity gradient with a reduced 'local' effective viscosity near the channel wall and the mild velocity gradient with an increased local effective viscosity in the center region. Since the clear fluid occupies only a thin lubrication layer next to the channel wall, the relative viscosity of the suspension is higher for a larger particle size although the 'local' effective viscosity is reduced in the lubrication layer.

In Fig. 8, the velocity profiles of the suspension for various volume fractions at $G/d = 10$ and $Re = 10$ are shown. The velocity distributions in this figure have been obtained by averaging the instantaneous values under the fully developed flow condition. $U_c$ is the centerline velocity of the standard Newtonian fluid with the same viscosity as the medium fluid but without particles for the applied pressure gradient under the fully developed flow condition. The velocity decreases as the volume fraction increases and the velocity profile of high volume fraction fluid is flatter than that of low volume fraction fluid at the center of the channel.

Apparently, the particles do not exhibit a uniform distribution in the fluid (i.e., parabolic velocity profile of the suspension) because the distribution of particles is affected by the flow of the medium fluid and vice versa. It is noteworthy that the particles under the Poiseuille flow condition are driven by the lift force, as reported by Patankar et al. (2001), acting in the radial direction from the wall to the center so that the particles are suspended at a distance off the wall. This radial displacement is due to the force caused by the shear stress distribution in the fluid. Segre and Silberberg's (1962b) experimental observation reported this phenomenon as the tubular pinch effect occurring in the laminar flow of suspensions of spherical particles through a circular tube. They argued that the particles are subject to radial displacements, outwards from the center of the tube and inwards from the wall. There existed an equilibrium radial position at about 0.6 times the radius from the axis around which the particles tend to cluster. In the present study, the number of the particles is much more than that of their experiment so that more frequent interactions among the particles occur, not considering the difference between a circular tube and a plane channel.

In Fig. 9, the velocity distributions of the suspension at $\Phi = 0.4$, whose relative viscosity is $\eta_r = 2.78$ (quoted for $G/d = 10$ from Fig. 7), are compared with that of the medium fluid without

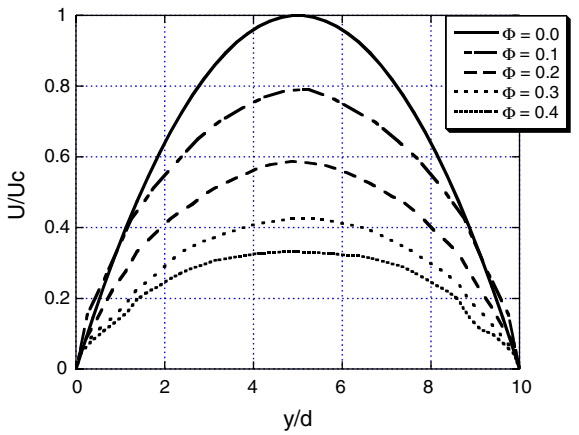


Fig. 8. Velocity profiles of the suspension with respect to the gapwise position for various volume fractions at $G/d = 10$ and $Re = 10$.

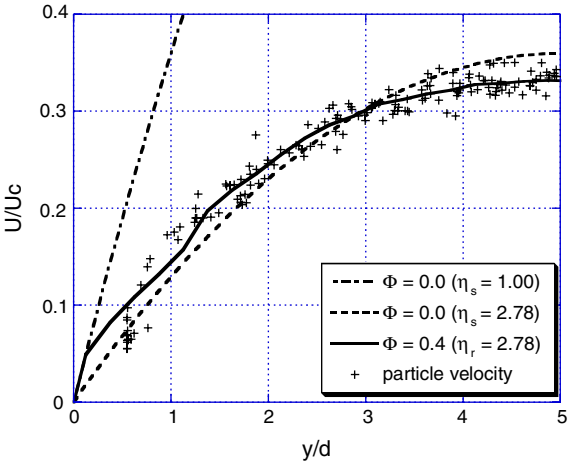


Fig. 9. Comparison of the velocity distribution of the suspension with that of the Newtonian fluid and the respective velocities of the particles along the gapwise direction at $G/d = 10$ and $Re = 10$.

particles having the same effective viscosity. The velocity of the suspension is slower than that of the fluid having the same effective viscosity without particles at the center while it is faster at the near-wall region, which shows the effect of the particles on the fluid motion.

In Fig. 10, the distributions of the particles in the channel with respect to the gapwise position for the suspension at $\Phi = 0.4$ and $Re = 10$ are shown for $G/d = 5$, 10 and 40. For $G/d = 5$ and 10, the particles are very sparsely distributed near the wall while they are aggregated densely in the center, giving the same results as Gavin (1997) who showed that the lift force could give rise to a reduced volume fraction adjacent to the duct wall in the laminar Poiseuille flow of ER and MR materials. He suggested that this locally diminished volume fraction reduces yield

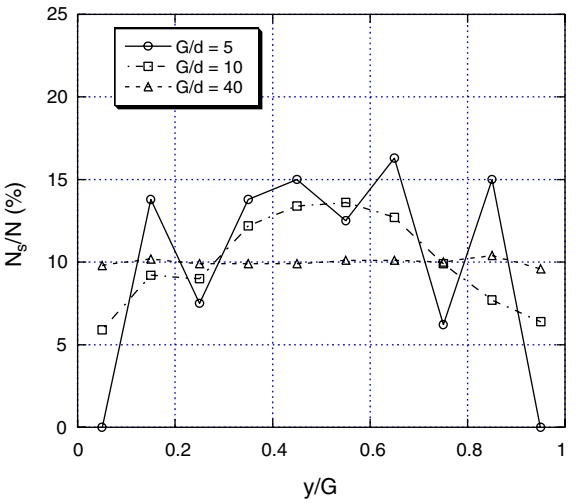


Fig. 10. Distribution of the particles along the gapwise direction for $G/d = 5$, 10 and 40 at $\Phi = 0.4$ and $Re = 10$.

stress near the duct boundaries, which can explain the observed reduction in dynamic yield stress as compared to static yield stress. However, at $G/d = 40$, the particles are almost uniformly distributed. This is because the wall effect is not so significant when the ratio of channel gap to particle diameter is large, resulting in small lift force from the wall even for a large volume fraction.

The non-uniform distribution of particles causes the non-uniform distribution of effective viscosity, which has an effect on the velocity profile in the flow. The reduced volume fraction adjacent to the wall reduces the effective viscosity, and the increased volume fraction at the center region makes the velocity profile there to be rather flat than parabolic. In Fig. 11, the numbers of particles in the sections throughout the channel gap for various volume fractions are shown. For the fluid of volume fraction $\Phi = 0.4$, the number of particles increases as the distance from the wall increases. However, for the cases of rather sparsely distributed fluid of volume fraction $\Phi = 0.05$, and $\Phi = 0.1$, the location at which particles are gathered close together is not at the center but shifted somewhat towards the wall. This distribution is corresponding to the tubular pinch effect reported by Segre and Silberberg (1962b). This result shows that the present DNS method can simulate the motion of particles to the minutest details efficiently.

In Fig. 12, snapshots of suspended particles and pressure distributions at the initial state and at the fully developed state for the fluid of volume fraction $\Phi = 0.1$ are shown. We can observe that the particles, which are placed at random positions initially, are aligned in two rows at a certain distance from the wall at the fully developed state. These snapshots are a manifestation of tubular pinch effect of the suspension.

The distribution of the particles is also affected by the Reynolds number. In Fig. 13, the distributions of the particles at $\Phi = 0.1$ with respect to the gapwise position at various Reynolds numbers are shown. At $Re = 5$, the distribution of the particles is similar to that at $Re = 10$. However, as the Reynolds number decreases, the distribution of the particles in the center region increases so that the tubular pinch effect decreases. This occurs because the forces that contribute to the radial displacement of particles are reduced as the Reynolds number decreases.

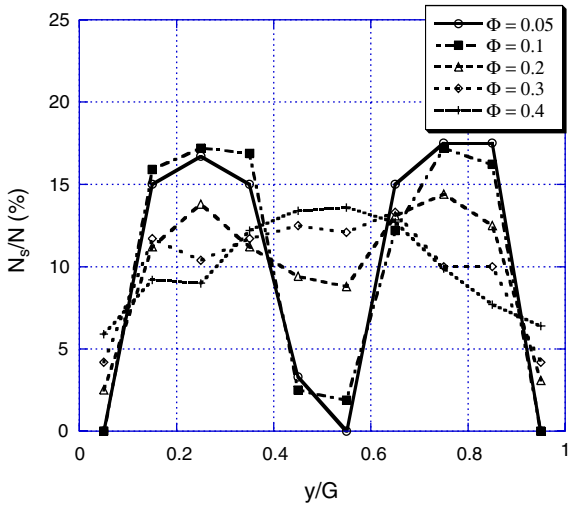


Fig. 11. Distribution of particles along the gapwise direction for various volume fractions at $G/d = 10$ and $Re = 10$.

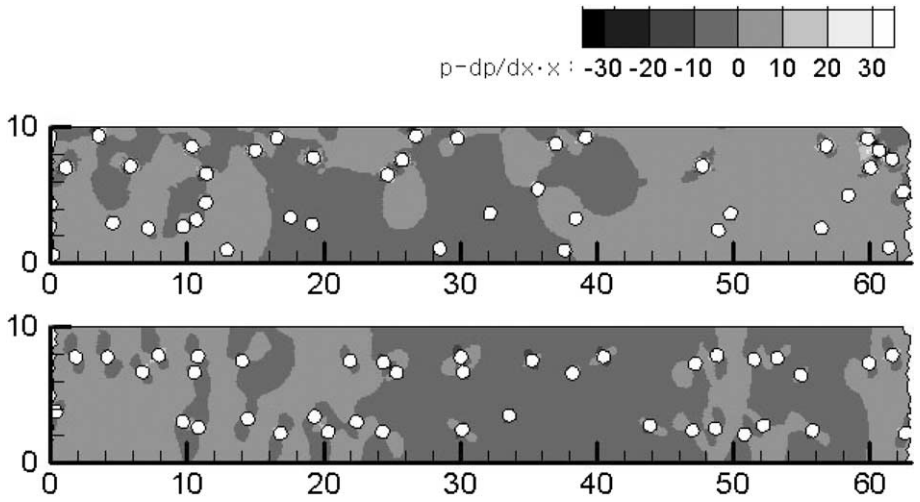


Fig. 12. Snapshots of the motion of particles and the pressure distribution at the initial state and at the fully developed state at $G/d = 10$, $\Phi = 0.05$, and $Re = 10$.

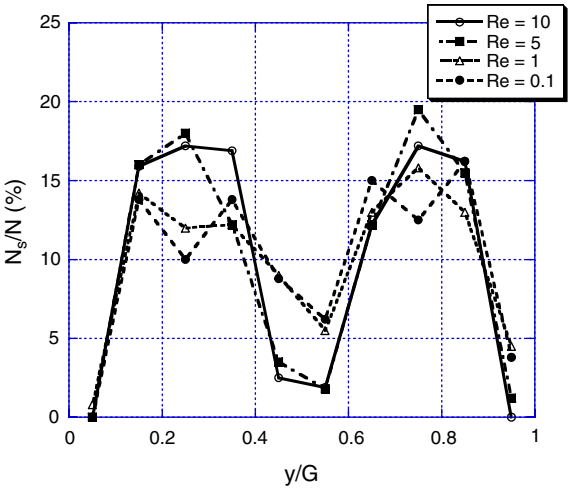


Fig. 13. Distribution of particles along the gapwise direction for various Reynolds numbers at $G/d = 10$ and $\Phi = 0.1$.

## 4. Conclusions

Two-dimensional channel flow of fluid laden with many particles is studied by direct numerical simulation using the Navier–Stokes equation for the fluid, coupled with Newton's law of motion for the particles.

The velocity profile and the distribution of the particles in the channel are shown for the fully developed flow condition. As the volume fraction increases at a fixed ratio of channel gap to particle diameter, the fluid velocity decreases, and the effective viscosity of suspension increases.

By comparing the relative viscosity of suspension directly calculated from the velocity distribution with previous results, it is discussed that the present simulation can realistically represent the resistance of the particle–laden fluid to flow. As the ratio of channel gap to particle diameter increases at a fixed volume fraction, the relative viscosity decreases.

The particles in the channel are displaced in the gapwise direction, inwards from the wall and outwards from the center. This tubular pinch effect observed in the previous experiment is substantiated by the present direct numerical simulation. The tubular pinch effect is enhanced as the Reynolds number increases, but it decreases when the volume fraction increases. The present DNS proves to be a useful tool for describing the fluid flow affected by particle interactions.

## Acknowledgment

This work has been supported by the Micro Thermal System Research Center of Seoul National University which is an ERC (Engineering Research Center) supported by the Korea Science and Engineering Foundation (KOSEF), and also by the Brain Korea 21 Project, Ministry of Education and Human Resources Development, Republic of Korea.

## References

Asmolov, E.S., 1999. The inertial lift on a spherical particle in a plane Poiseuille flow at large channel Reynolds number. J. Fluid Mech. 381, 63–87.

Batchelor, G.K., 1977. The effect of Brownian motion on the bulk stress in a suspension of spherical particles. J. Fluid Mech. 83, 97–117.

Brady, J.F., 1984. The Einstein viscosity correction in n dimensions. Int. J. Multiphase Flow 10, 113–114.

Cherukat, P., McLaughlin, J.B., 1994. The inertial lift on a rigid sphere in a linear shear flow field near a flat wall. J. Fluid Mech. 263, 1–18.

Cherukat, P., McLaughlin, J.B., Dandy, D.S., 1999. A computational study of the inertial lift on a sphere in a linear shear flow field. Int. J. Multiphase Flow 25, 15–33.

Choi, H.G., 2000. Splitting method for the combined formulation of the fluid–particle problem. Comput. Methods Appl. Mech. Eng. 190, 1367–1378.

Choi, H.G., Choi, H., Yoo, J.Y., 1997. A fractional four-step finite element formulation of the unsteady incompressible Navier–Stokes equations using SUPG and linear equal-order element methods. Comput. Methods Appl. Mech. Eng. 143, 333–348.

Choi, H.G., Joseph, D.D., 2001. Fluidization by lift of 300 circular particles in plane Poiseuille flow by direct numerical simulation. J. Fluid Mech. 438, 101–128.

Dandy, D.S., Dwyer, H.A., 1990. A sphere in shear flow at finite Reynolds number: Effect of shear on particle lift, drag and heat transfer. J. Fluid Mech. 216, 381–410.

Dodd, T.L., Hammer, D.A., Sangani, A.S., Koch, D.L., 1995. Numerical simulations of the effect of hydrodynamic interactions on diffusivities of integral membrane proteins. J. Fluid Mech. 293, 147–180.

Einstein, A., 1906. A new determination of molecular dimensions. Annalen der Physik 19, 289.

Feng, Z.-G., Michaelides, E.E., 2003. Equilibrium position for a particle in a horizontal shear flow. Int. J. Multiphase Flow 29, 947–957.

Gavin, H.P., 1997. The effect of particle concentration inhomogeneities on the steady flow of electro- and magneto-rheological materials. J. Non-Newtonian Fluid Mech. 71, 165–182.

Hesla, T.I., 1991. Combined formulation of fluid–particle problem, unpublished note.

Hogg, A.J., 1994. The inertial migration of non-neutrally buoyant spherical particles in two dimensional flows. J. Fluid Mech. 272, 285–318.

Hu, H.H., 1996. Direct simulation of flows of solid–liquid mixtures. Int. J. Multiphase Flow 22, 335–352.

Hu, H.H., Joseph, D.D., Crochet, M.J., 1992. Direct simulation of fluid particle motions. Theor. Comput. Fluid Dynamics 3, 285–306.

Kataoka, T., Kitano, T., Sasahara, M., Nishijima, K., 1978. Viscosity of particle filled polymer melts. Rheol. Acta 17, 149–155.

Kurose, R., Komori, S., 1999. Drag lift forces on a rotating sphere in a linear shear flow. J. Fluid Mech. 384, 183–206.

Patankar, N.A., Huang, P.Y., Ko, T., Joseph, D.D., 2001. Lift-off of a single particle in Newtonian and viscoelastic fluids by direct numerical simulation. J. Fluid Mech. 438, 67–100.

Prosperetti, A., 2004. Average stress in a Stokes suspension of disks. Int. J. Multiphase Flow 30, 1–26.

Segre, G., Silberberg, A., 1962a. Behavior of macroscopic rigid spheres in Poiseuille flow Part 1. Determination of local concentration by statistical analysis of particle passages through crossed light beams. J. Fluid Mech. 14, 115.

Segre, G., Silberberg, A., 1962b. Behavior of macroscopic rigid spheres in Poiseuille flow Part 2. Experimental results and interpretation. J. Fluid Mech. 14, 136.